Post-transplant molecularly defined Burkitt lymphomas are frequently *MYC*-negative and characterized by the 11q-gain/loss pattern

Julio Finalet Ferreiro,[1] Julie Morscio,[2] Daan Dierickx,[3] Lukas Marcelis,[2] Gregor Verhoef,[3] Peter Vandenberghe,[1] Thomas Tousseyn,[2] and Iwona Wlodarska[1]

[1]*KU Leuven, University of Leuven, Center for Human Genetics;* [2]*KU Leuven, University of Leuven, Translational Cell and Tissue Research and KU Leuven, University Hospitals Leuven, Department of Pathology; and* [3]*KU Leuven, University Hospitals Leuven, Department of Hematology, Belgium*

Supplementary information

Supplementary Methods

Cytogenetics and FISH

G-banding chromosomal analysis and fluorescence *in situ* hybridization (FISH) followed routine methods. DNA probes, Bacterial Artificial Clones (BAC), applied for FISH were selected from www.Oct29012.archive.ensembl.org (Supplementary Figure 2). The probes were labeled with SpectrumOrange- and SpectrumGreen-d-UTP (Abbott Molecular, Ottigne, Belgium) using random priming. FISH images were acquired with a fluorescence microscope equipped with an Axiophot 2 camera (Carl Zeiss Microscopy, Jena, Germany) and a MetaSystems ISIS imaging system (MetaSystems, Altlussheim, Germany). In each experiment up to 8 abnormal metaphases and/or 200 interphase cells were evaluated.

High resolution array Comparative Genome Hybridization (aCGH)

Total genomic DNA was isolated from fresh frozen lymphoma samples using standard procedures. Genomic profiling, following the manufacturer's protocols, was performed using the Affymetrix Cytogenetic array 2.7M (www.affymetrix.com). The initial data analysis was performed with the software "Chromosome Analysis Suit" (CHAS) and subsequent analysis (segmentation and aberration heatmap) were performed using the software "ArrayStudio" (www.omicsoft.com). Array CGH data are available at GEO (http://www.ncbi.nlm.nih.gov/projects/geo/query/acc.cgi?acc=GSE64086).

Gene Expression profiling and pathway analysis

Total RNA extraction was performed using TRIzol LS Reagent (Life Technologies Europe B.V., Gent, Belgium). The HG-U133 Plus 2.0 Affymetrix platform (www.affymetrix.com) was used and the raw data (CEL files) were normalized using the GeneChip-Robust Multiarray Averaging (GC-RMA) algorithm. Hierarchical clustering was applied to detect relationship in the data and to identify outliers. To find differentially expressed genes, the General Linear Model (GLM) module of ArrayStudio was used for inference analysis. (www.omicsoft.com). Gene expression data are available at GEO (http://www.ncbi.nlm.nih.gov/projects/geo/query/acc.cgi?acc=GSE64086).

The cases were classified using two molecular gene signatures of BL described by Hummel *et al.* 2006[1] and Dave *at al.* 2006.[2] As a control group, we selected 29 previously studied cases of DLBCL

which were analyzed with the same Affymetrix platform.[3] To group the cases using hierarchical clustering, we used the Ward and Manhattan methods for the linkage and distance, respectively. The clustering of the probes was done using complete link and Pearson's correlation (see details: http://www.arrayserver.com/wiki/index.php?title=HierarchicalClustering).

To identify 11q genes dysregulated in ID-BL with 11q-gain/loss pattern (11q+/-), we performed inference analysis comparing three cases with 11q+/- *versus* four cases of *MYC*-translocation positive BL (t(MYC)). To find significant enriched pathways and biological functions in ID-BL with 11q+/-, we uploaded the result of the inference analyses into the "Ingenuity Pathway Analysis" application (IPA, www.ingenuity.com). From the three confidence levels provided by the system, we used "Experimentally observed" and "Highly predicted" data. For details see:

http://ingenuity.force.com/ipa/articles/Tutorial/Tutorials.

Statistical analysis

Association between categorical variables was tested by the Fisher's exact test. *P*-value <0.005 was considered statistically significant.

Immunohistochemistry and chromogenic in situ hybridization

Immunohistochemical stainings were performed on paraffin-embedded sections. All antisera were ready to use antibodies purchased from DAKO (DAKO, Carpinteria, USA) except for C-MYC (Y69, Epitomics, Abcam, Burlingame, CA, USA) and stained in automated fashion according to the manufacturer's recommendations. IHC results were visualized using the OptiView DAB IHC Detection Kit (Ventana, Oro Valley, Tucson, Arizona). Image acquisition was done through a Leica microscope at 200x and 100x magnification. Images were assembled using Adobe Photoshop CS5.

Chromogenic EBER (EBV-encoded RNA) in situ hybridization is considered the standard for diagnosis of EBV-infection and was performed using a 30-mer digoxigenin-labeled oligonucleotide probe (Research Genetics, Huntsville, AL), according to manufacturer's instructions. A control poly-A probe (Ventana Roche, Arizona USA) was used to check for RNA integrity and a proven EBV-driven lymphoma was used as a positive control.

Supplementary references

1. Hummel M, Bentink S, Berger H, et al. A biologic definition of Burkitt's lymphoma from transcriptional and genomic profiling. N Engl J Med. 2006;354(23):2419-2430.

2. Dave SS, Fu K, Wright GW, et al. Molecular diagnosis of Burkitt's lymphoma. N Engl J Med. 2006;354(23):2431-2442.

3. Morscio J, Dierickx D, Ferreiro JF, et al. Gene expression profiling reveals clear differences between EBV-positive and EBV-negative posttransplant lymphoproliferative disorders. Am J Transplant. 2013;13(5):1305-1316.

4. Salaverria I, Martin-Guerrero I, Wagener R, et al. A recurrent 11q aberration pattern characterizes a subset of MYC-negative high-grade B-cell lymphomas resembling Burkitt lymphoma. Blood. 2014;123(8):1187-1198.

Supplementary Figure 1
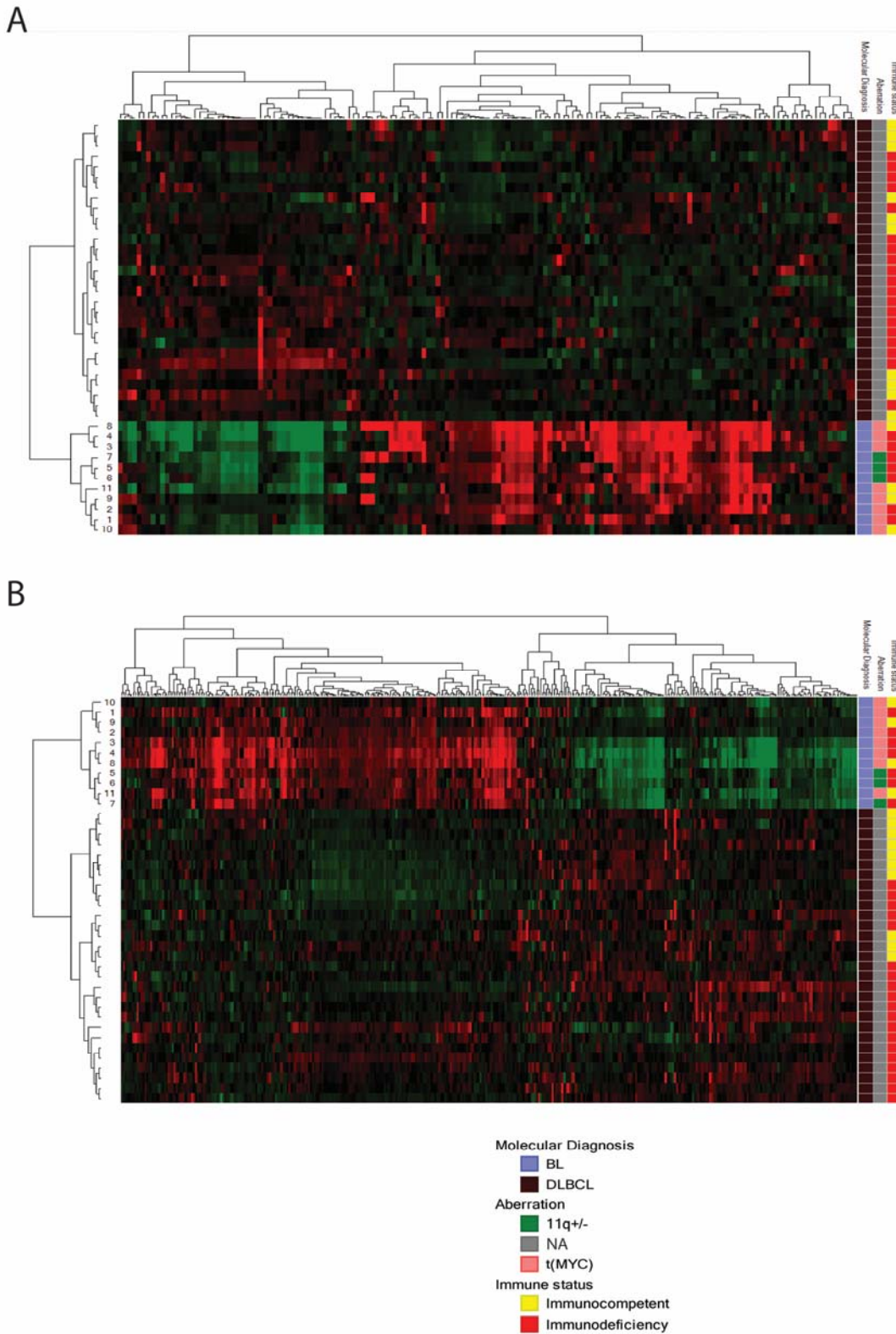
Supplementary Figure S1. Validation of the molecular features of 11 studied BL cases. Hierarchical clustering using the BL signatures from Hummel *et al*. 2006[1] (A) and Dave et al.[2] (B). All cases clustered together and were separated from 19 IC-DLBCL and 10 PT-DLBCL.[3] These data were collected from our microarray experiment in which we used the HG-U133 Plus 2.0 Affymetrix platform. In this platform the gene annotation is based on the genome build Hg19.

Supplementary Figure 2
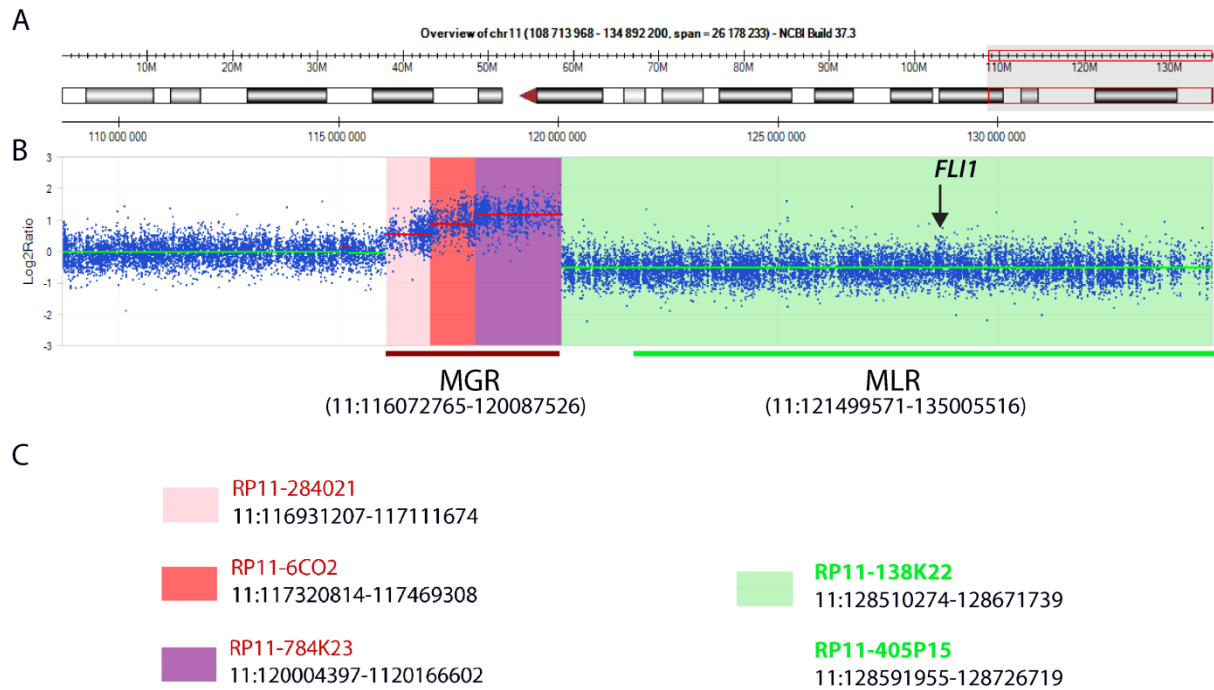
Supplementary Figure S2. Design of the 11q-MGR/MLR FISH assay. (A) View of chromosome 11 with the indicated 11q23.3qter region; (B) 11q imbalances detected by aCGH in case 6, which showed the smallest region of gain (~4 Mb); (C) Selected bacterial artificial chromosome (BAC) clones (www.Oct2012.archive.ensembl.org) and their genomic localization. Note that the assay comprises three MGR-related BAC clones (labeled with SpectrumOrange-d-UTP, shown in red-scale) representing three differentially gained areas in case 6 and two clones spanning *FLI1* (labeled with SpectrumGreen-d-UTP, shown in green), the gene targeted by biallelic deletion on one case reported by Salaverria et al.[4]

Supplementary Figure 3
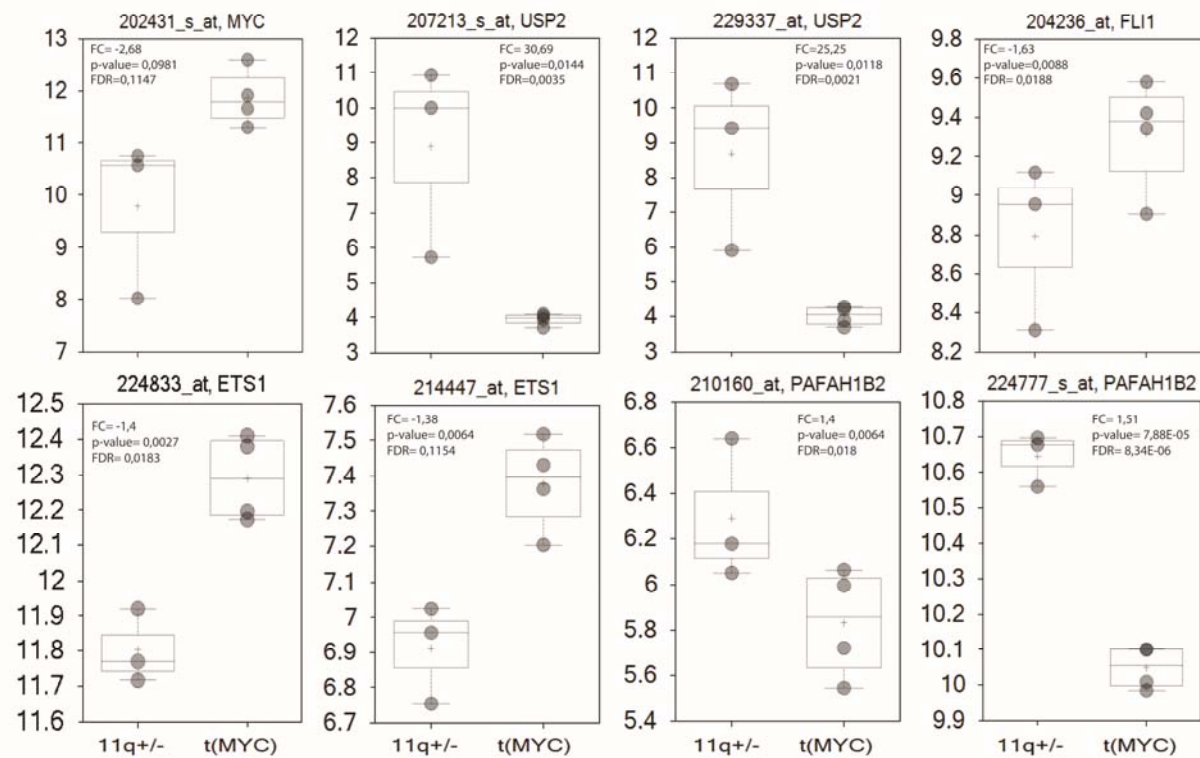
Supplementary Figure S3. Expression value of selected genes. Normalized signal values of array probes covering *USP2, ETS1, PAFAH1B2, FLI1* and *MYC*. The p-value and the "corrected-for-multiple-testing" p-value (FDR) are provided for the individual probes.

Supplementary Figure 4
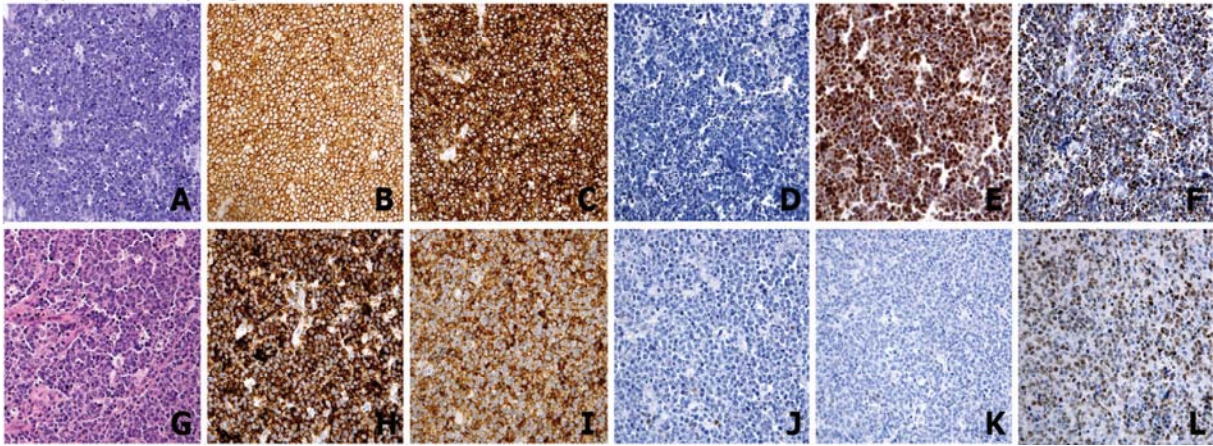
Supplementary Figure S4. Morphology and immunophenotype of ID-mBL. Images in the top and bottom rows represent *MYC*-translocation-positive case 4 and case 5 with the 11q-gain/loss pattern, respectively. (A) and (G), hematoxilin&eosin staining. In the remaining images, examples of immunohistochemistry for CD20 (B and H), CD10 (C and I), BCL2 (D and J), MYC (E and K) and Ki67 (F and L). The images were taken at 200x and then scaled.

Supplemental Table S1. Differentially expressed genes in MGR (red) and MLR (green).

probe set id	Gene Symbol	Gene Title	11q+/- vs t[MYC] FoldChange	11q+/- vs t[MYC] PValue	Chromosome	Start	End	Chromosomal band
224777_s_at	PAFAH1B2	platelet-activating factor acetylhydrolase 1b, catalytic subunit 2 (30kDa)	1,5121	7,88E-05	chr11	117015043	117041759	chr11q23
202038_at	UBE4A	ubiquitination factor E4A	2,1626	0,0335	chr11	118230358	118269922	chr11q23.3
208745_at	ATP5L	ATP synthase, H+ transporting, mitochondrial Fo complex, subunit G	1,8159	0,0432	chr11	118272103	118280562	chr11q23.3
208746_x_at	ATP5L	ATP synthase, H+ transporting, mitochondrial Fo complex, subunit G	1,5583	0,0282	chr11	118272320	118279908	chr11q23.3
210453_x_at	ATP5L	ATP synthase, H+ transporting, mitochondrial Fo complex, subunit G	1,5499	0,0342	chr11	118272321	118279914	chr11q23.3
207573_x_at	ATP5L	ATP synthase, H+ transporting, mitochondrial Fo complex, subunit G	1,5705	0,0358	chr11	118272330	118279910	chr11q23.3
218483_s_at	IFT46	intraflagellar transport 46 homolog (Chlamydomonas)	2,3249	0,0091	chr11	118415260	118436714	chr11q23.3
201176_s_at	ARCN1	archain 1	2,7523	0,0114	chr11	118443147	118473613	chr11q23.3
225549_at	DDX6	DEAD (Asp-Glu-Ala-Asp) box helicase 6	1,3804	0,0222	chr11	118500744	118620182	chr11q23.3
227208_at	CCDC84	coiled-coil domain containing 84	2,6342	0,0394	chr11	118883892	118889035	chr11q23.3
200091_s_at	RPS25	ribosomal protein S25	1,3548	0,0359	chr11	118886429	118889326	chr11q23.3
203292_s_at	VPS11	vacuolar protein sorting 11 homolog (S. cerevisiae)	2,2357	0,0177	chr11	118938492	118952675	chr11q23
213344_s_at	H2AFX	H2A histone family, member X	1,8155	0,0209	chr11	118964583	118965076	chr11q23.3
205436_s_at	H2AFX	H2A histone family, member X	2,0447	0,0427	chr11	118964586	118966177	chr11q23.3
204757_s_at	C2CD2L	C2CD2-like	1,71	0,0475	chr11	118978783	118989043	chr11q23.3
206495_s_at	HINFP	histone H4 transcription factor	3,211	0,0171	chr11	118997642	119005764	chr11q23.3
1553695_a_at	NLRX1	NLR family member X1	2,2767	0,021	chr11	119039439	119054725	chr11q23.3
219680_at	NLRX1	NLR family member X1	2,2785	0,0016	chr11	119045428	119054723	chr11q23.3
229010_at	CBL	Cbl proto-oncogene, E3 ubiquitin protein ligase	2,6837	0,0246	chr11	119171132	119172744	chr11q23.3
225231_at	CBL	Cbl proto-oncogene, E3 ubiquitin protein ligase	2,0956	0,0272	chr11	119175481	119178857	chr11q23.3
225234_at	CBL	Cbl proto-oncogene, E3 ubiquitin protein ligase	1,9879	0,0279	chr11	119175481	119178857	chr11q23.3
229337_at	USP2	ubiquitin specific peptidase 2	25,2497	0,0118	chr11	119225924	119226401	chr11q23.3
207211_at	USP2	ubiquitin specific peptidase 2	1,372	0,0399	chr11	119227511	119234629	chr11q23.3
207213_s_at	USP2	ubiquitin specific peptidase 2	30,6986	0,0144	chr11	119227511	119234629	chr11q23.3
204327_s_at	ZNF202	zinc finger protein 202	-2,0264	0,0086	chr11	123594634	123612325	chr11q23.3
204329_s_at	ZNF202	zinc finger protein 202	-1,7887	0,034	chr11	123594634	123612325	chr11q23.3
225819_at	TBRG1	transforming growth factor beta regulator 1	-1,6264	0,0219	chr11	124492773	124502634	chr11q24.2
230320_at	TBRG1	transforming growth factor beta regulator 1	-1,4489	0,0304	chr11	124504861	124505294	chr11q24.2
235654_at	TMEM218	transmembrane protein 218	-1,6734	0,0319	chr11	124965539	124966001	chr11q24.2
226073_at	TMEM218	transmembrane protein 218	-1,6272	0,024	chr11	124966576	124981604	chr11q24.2
208289_s_at	EI24	etoposide induced 2.4 mRNA	-1,6532	0,0395	chr11	125439411	125454575	chr11q24
216396_s_at	EI24	etoposide induced 2.4 mRNA	-1,7454	0,0167	chr11	125452532	125454124	chr11q24
202223_at	STT3A	STT3, subunit of the oligosaccharyltransferase complex, homolog A (S. cerevisiae)	-1,9276	0,0081	chr11	125462741	125490953	chr11q23.3
221277_s_at	PUS3	pseudouridylate synthase 3	-1,9179	0,004	chr11	125763379	125766209	chr11q24.2
225398_at	RPUSD4	RNA pseudouridylate synthase domain containing 4	-2,1666	0,0062	chr11	126071990	126081531	chr11q24.2
223386_at	FAM118B	family with sequence similarity 118, member B	-1,5259	0,0477	chr11	126081698	126132460	chr11q24.2
223128_at	FOXRED1	FAD-dependent oxidoreductase domain containing 1	-1,8328	0,0025	chr11	126139054	126148026	chr11q24.2
1552804_a_at	TIRAP	toll-interleukin 1 receptor (TIR) domain containing adaptor protein	-1,4053	0,0153	chr11	126153001	126163130	chr11q24.2
218774_at	DCPS	decapping enzyme, scavenger	-2,0301	0,0227	chr11	126173969	126215644	chr11q24.2
224833_at	ETS1	v-ets erythroblastosis virus E26 oncogene homolog 1 (avian)	-1,402	0,0027	chr11	128328659	128332010	chr11q23.3
1555355_a_at	ETS1	v-ets erythroblastosis virus E26 oncogene homolog 1 (avian)	-1,3274	0,0412	chr11	128331389	128392160	chr11q23.3
214447_at	ETS1	v-ets erythroblastosis virus E26 oncogene homolog 1 (avian)	-1,3826	0,0064	chr11	128332071	128392248	chr11q23.3
214875_x_at	APLP2	amyloid beta (A4) precursor-like protein 2	-1,6967	0,049	chr11	129979330	130014283	chr11q24
202005_at	ST14	suppression of tumorigenicity 14 (colon carcinoma)	-1,9629	0,0261	chr11	130029839	130080256	chr11q24-q25
216905_s_at	ST14	suppression of tumorigenicity 14 (colon carcinoma)	-2,0863	0,0067	chr11	130058086	130080256	chr11q24-q25
226148_at	ZBTB44	zinc finger and BTB domain containing 44	-1,8138	0,0349	chr11	130100253	130131329	chr11q24.3
220243_at	ZBTB44	zinc finger and BTB domain containing 44	-2,3587	0,0376	chr11	130108974	130184321	chr11q24.3
202358_s_at	SNX19	sorting nexin 19	-1,3925	0,0414	chr11	130745773	130786362	chr11q25
202359_s_at	SNX19	sorting nexin 19	-1,5302	0,048	chr11	130745774	130786362	chr11q25
1554986_a_at	SNX19	sorting nexin 19	-1,4202	0,0304	chr11	130775552	130786344	chr11q25
212789_at	NCAPD3	non-SMC condensin II complex, subunit D3	-1,6052	0,0363	chr11	134022339	134093868	chr11q25
221669_s_at	ACAD8	acyl-CoA dehydrogenase family, member 8	-1,3771	0,0254	chr11	134123464	134135555	chr11q25